

A STUDY OF FRESNEL SCATTERED FIELD FOR NON-SPHERICAL DISCRETE SCATTERERS

H. T. Ewe and H. T. Chuah

Faculty of Engineering
Multimedia University
Bukit Beruang, 75450
Melaka, Malaysia

1. Introduction

2. Formulation

2.1 Fresnel Zone Consideration

2.2 Scattered Fields of Disk-shaped and Needle-shaped Scatterers

2.3 Scattered Fields of Cylindrical Scatterers

3. Theoretical Analysis

3.1 Disk

3.2 Needle

3.3 Cylinder

4. Comparisons with Measurement Data

5. Conclusion

Appendix

References

1. INTRODUCTION

For decades, researchers have been pursuing on the study of the interaction between electromagnetic waves and simple physical objects such as spheres, ellipsoids and cylinders. The internal field of an ellipsoid due to a uniform and parallel incident field was studied by [1]. For ellipsoids with very transparent material where the refractive index is very small and the size is small compared with wavelength, the Rayleigh-Gans approximation can be applied to calculate the scattered

field [2]. In this method, it is assumed that each volume element in the object gives Rayleigh scattering independently and the total scattered field is obtained by integrating the scattered fields from all volume elements with the inclusion of the relative phase contributions due to their positions. This method is extended in [3] by considering the generalized Rayleigh-Gans (GRG) approximation. This approximation is applicable for nontenuous ellipsoids with at least one of its dimensions small compared with the wavelength. In this case, disk and needle shaped scatterers can be considered as they can be approximated by thin oblate spheroids and long prolate spheroids, respectively. The generalized Rayleigh-Gans approximation was applied in [4] in their study of electromagnetic wave scattering from vegetation samples. For the cylindrical scatterers, the problem of a normal incidence plane wave scattered by an infinitely long circular cylinder was first solved and discussed by Rayleigh [5, 6], and the oblique incidence case was later solved by Wait [6, 7]. In the study of electromagnetic scattering from a layer of dielectric circular cylinders, the scattering solution of infinitely long cylinder was adapted in [8] to apply to cylinders with finite length.

In these papers, far field approximation of the scattered field is assumed. However, when the scatterers are in the Fresnel zone of one another, it is necessary to include this additional interaction effect in the scattered field of the scatterers. A study on the Fresnel field interaction between the close-spaced scatterers for disks and needles was carried out in [9] where the Fresnel phase correction and the amplitude correction to the far field scattered field were included. The detailed expressions of these corrections are also found in [10] where additional Fresnel zone higher order term is added. In this study, both the phase and the amplitude corrections of the scattered fields of disks and needles described in [10] are considered. In addition, the concept is extended in this paper to cover the case of finite length cylinder where the expressions of the phase and the amplitude corrections of the scattered fields of finite length cylinders are developed. A geometrical discussion of the need of these corrections for the scatterers in the Fresnel zone of one another is also presented. From the theoretical analysis of the effects of these corrections to the scattering cross section of disks, needles and cylinders, it is found that the amplitude and the Fresnel phase corrections are generally required when the Fresnel factor is larger than $\frac{\pi}{8}$. The Fresnel factor is defined as $\frac{ka^2}{2d}$ for disks

and $\frac{kh^2}{2d}$ for needles and cylinders where a and h are the radius of disks and the half-length of needles and cylinders, respectively. The calculated scattering cross sections with both amplitude and Fresnel phase corrections for rods, disks, birch stick and aspen leaf are found to be in good agreement with the measurement results.

2. FORMULATION

2.1 Fresnel Zone Consideration

Consider a time-harmonic plane wave impinging upon a scatterer in the local frame,

$$\bar{E}_{il}(\bar{r}) = \hat{q}_{il} E_o e^{-jk\hat{i}'' \cdot \bar{r}} \quad (1)$$

where E_o is the amplitude of the incident field and k is the wave number of the background medium. The time dependence term $e^{j\omega t}$ is assumed and suppressed. \hat{i}'' is the unit vector in the incident direction and the polarization unit vector \hat{q}_{il} can be \hat{v}_{il} or \hat{h}_{il} . These unit vectors can be expressed by the local polar and azimuthal angles θ_{il} , ϕ_{il} , θ_{sl} , ϕ_{sl} as shown below:

$$\begin{aligned} \hat{i}'' &= \hat{x}'' \sin \theta_{il} \cos \phi_{il} + \hat{y}'' \sin \theta_{il} \sin \phi_{il} + \hat{z}'' \cos \theta_{il} \\ \hat{h}_{il} &= \frac{\hat{z}'' \times \hat{i}''}{|\hat{z}'' \times \hat{i}''|} = -\hat{x}'' \sin \phi_{il} + \hat{y}'' \cos \phi_{il} \\ \hat{v}_{il} &= \hat{h}_{il} \times \hat{i}'' = \hat{x}'' \cos \theta_{il} \cos \phi_{il} + \hat{y}'' \cos \theta_{il} \sin \phi_{il} - \hat{z}'' \sin \theta_{il} \end{aligned} \quad (2)$$

The same set of unit vectors for scattered direction can also be derived as shown below:

$$\begin{aligned} \hat{s}'' &= \hat{x}'' \sin \theta_{sl} \cos \phi_{sl} + \hat{y}'' \sin \theta_{sl} \sin \phi_{sl} + \hat{z}'' \cos \theta_{sl} \\ \hat{h}_{sl} &= \frac{\hat{z}'' \times \hat{s}''}{|\hat{z}'' \times \hat{s}''|} = -\hat{x}'' \sin \phi_{sl} + \hat{y}'' \cos \phi_{sl} \\ \hat{v}_{sl} &= \hat{h}_{sl} \times \hat{s}'' = \hat{x}'' \cos \theta_{sl} \cos \phi_{sl} + \hat{y}'' \cos \theta_{sl} \sin \phi_{sl} - \hat{z}'' \sin \theta_{sl} \end{aligned} \quad (3)$$

For the scattered field from a scatterer in the local frame, it is given by the integral representation below [10]:

$$\hat{p}_{sl} \cdot \bar{E}_{sl}(\bar{r}) = \frac{k^2(\epsilon_r - 1)}{4\pi} \int_{V''} \frac{\exp(-jk|\bar{r} - \bar{r}''|)}{|\bar{r} - \bar{r}''|} (\hat{p}_{sl} \cdot \bar{E}_{int}) d\bar{r}'' \quad (4)$$

where \bar{E}_{int} is the internal field of the scatterer, \hat{p}_{sl} the scattered polarization unit vector in the local frame and \bar{r} the local frame location vector at the observation point. The vector \bar{r}'' is the local frame location vector for the volume element in the scatterer and V'' refers to the volume of the scatterer.

To specialize the scattered field expression to the Fresnel zone, we first consider the $|\bar{r} - \bar{r}''|$ term in (4) and express it in the following form [11],

$$|\bar{r} - \bar{r}''| = \sqrt{r^2 - 2\bar{r} \cdot \bar{r}'' + r''^2} = r \sqrt{1 + \left(-\frac{2\bar{r} \cdot \bar{r}''}{r^2} + \frac{r''^2}{r^2} \right)} \quad (5)$$

Assuming the terms with the denominator r^2 are small compared with unity and by using the expression of $(1+x)^{\frac{1}{2}} \approx 1 + \frac{x}{2} - \frac{x^2}{8}$, the $|\bar{r} - \bar{r}''|$ term in (5) can be approximated to give

$$\begin{aligned} |\bar{r} - \bar{r}''| &\approx r - \hat{s}'' \cdot \bar{r}'' + \frac{r''^2}{2r} \left[1 - (\hat{s}'' \cdot \hat{r}'')^2 + \frac{(\hat{s}'' \cdot \bar{r}'')}{r} - \frac{r''^2}{4r^2} \right] \\ &\approx r - \hat{s}'' \cdot \bar{r}'' + \frac{r''^2}{2r} [1 - (\hat{s}'' \cdot \hat{r}'')^2] \end{aligned} \quad (6)$$

where $\hat{s}'' = \frac{\bar{r}}{r}$, $\hat{r}'' = \frac{\bar{r}''}{r''}$ and the last two terms in the square brackets have been neglected. The approximation in (6) which includes the Fresnel zone expression $\frac{r''^2}{2r} [1 - (\hat{s}'' \cdot \hat{r}'')^2]$ will be used for the exponential term $|\bar{r} - \bar{r}''|$ in the scattered field expression.

For the denominator term $|\bar{r} - \bar{r}''|$ in (4), which is not a phase term, it can be approximated by considering only the first two terms of (6) as shown below:

$$\frac{1}{|\bar{r} - \bar{r}''|} \approx \frac{1}{r - \hat{s}'' \cdot \bar{r}''} \approx \frac{1}{r} \left(1 + \frac{\hat{s}'' \cdot \bar{r}''}{r} \right) \quad (7)$$

For the generalized Rayleigh-Gans method used in [4], only the first two terms of (6) are considered in the exponential term in (4) and

the denominator term $|\bar{r} - \bar{r}''|$ is approximated to be r . In [9], the expression of $|\bar{r} - \bar{r}''| \approx r - \hat{s}'' \cdot \bar{r}'' + \frac{r''^2}{2r}$ was considered in the exponential term and the approximation in (7) was used for the denominator term.

To understand the corrections needed in the phase term in (4) for the inclusion of near field effects in the scattered field, a simple scattering geometry of a scatterer is shown in Figure 1. The needle-shaped scatterer is chosen to provide a better understanding of the near field effects for different observation angles.

When the observation point is at far field from the scatterer, it is reasonable to consider that the scattered vector for point O of the scatterer (\bar{r} or \overline{OC}) and that of point $B(\bar{r}_{\parallel})$ are parallel to each other. Point B can be any point in the scatterer. Thus, the relative phase difference of the scattered fields from points O and B to the observation point in far field can be considered by knowing the distance OA ($OA = r'' \cos \vartheta = \frac{\bar{r}}{r} \cdot \bar{r}'' = \hat{s}'' \cdot \bar{r}''$). The distance from point B to the observation point is then given by $r - \hat{s}'' \cdot \bar{r}''$.

However, when the observation point (in this case, C) is near to the scatterer as in the case of closely spaced scatterers, it is no longer proper to consider that the scattered fields from points O and B are in parallel. Instead, the distance between points B and C is given by $|\bar{r} - \bar{r}''|$, which is the term considered in (4). From the geometry plotted in Figure 1, it is shown that

$$|\bar{r} - \bar{r}''| = r_2 + r_3 = r_1 + r_3 = r - r'' \cos \vartheta + r_3 = r - \hat{s}'' \cdot \bar{r}'' + r_3 \quad (8)$$

where r_2 is chosen to be equal to r_1 . It is found that the terms $r - \hat{s}'' \cdot \bar{r}''$ are the same as the first two terms in (6) and represent the distance from point B to the observation point in far location. Thus, the term r_3 is the first order correction term needed when the observation point is close to the scatterer.

To obtain the expression of r_3 , we first consider the triangle ABC and get the following expression:

$$(r_2 + r_3)^2 = r_1^2 + (r'' \sin \vartheta)^2 \quad (9)$$

Since $r_2 = r_1$, equation (9) can be simplified to give a quadratic equation $r_3^2 + 2r_1 r_3 - r''^2 \sin^2 \vartheta = 0$, which can be solved to give

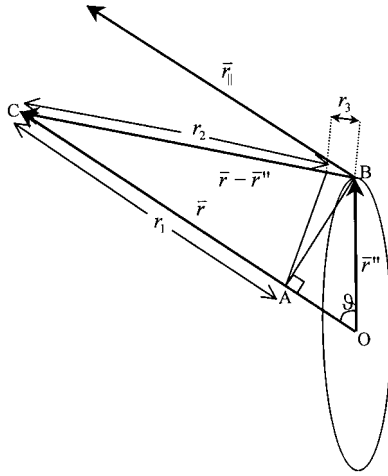


Figure 1. Scattering geometry of a scatterer for consideration of near field effect.

$$r_3 = -r_1 \pm \sqrt{r_1^2 + r''^2 \sin^2 \vartheta} = -r_1 \pm r_1 \sqrt{1 + \frac{r''^2 \sin^2 \vartheta}{r_1^2}} \quad (10)$$

As the distance r_3 must be positive, positive root is chosen. After using the expansion $(1 + x)^{\frac{1}{2}} \approx 1 + \frac{x}{2}$, the distance r_3 is given by

$$r_3 \approx \frac{r''^2 \sin^2 \vartheta}{2r} \left(1 + \frac{r'' \cos \vartheta}{r} + \text{higher order terms} \right) \quad (11)$$

Knowing that r'' is generally smaller than r for the whole scatterer and $\cos \vartheta$ is maximum when $\sin^2 \vartheta$ is zero, the rest of the terms in the bracket can be ignored except the unity term. Equation (11) becomes

$$r_3 \approx \frac{r''^2 \sin^2 \vartheta}{2r} \approx \frac{r''^2}{2r} [1 - (\hat{s}'' \cdot \hat{r}'')^2] \quad (12)$$

where the expression $\sin^2 \vartheta = 1 - \cos^2 \vartheta = 1 - (\hat{s}'' \cdot \hat{r}'')^2$ has been used. Thus, by comparing (12) and (6), it is known that the additional Fresnel term in (6) is actually the approximated term introduced to take into account the near field effect of the scattered field. From the expression in equation (12), it is known that the Fresnel term is important

when the angle $\vartheta \rightarrow 90^\circ$ and becomes zero at $\vartheta = 0^\circ, 180^\circ$. However, the Fresnel term is also dependent on r''^2 , thus in the scatterer with one dimension much smaller than the other dimension, such as needle-shaped scatterers, the contribution to the Fresnel term from the larger dimension of the scatterer is generally more important than that of the shorter dimension.

Referring to (4), since the term $\frac{r''^2}{2r}[1 - (\hat{s}'' \cdot \hat{r}'')^2]$ in (6) is to be combined with the wavenumber k to give the Fresnel phase term, it is possible to predict the range where this term is contributing to the scattered field which cannot be neglected. Generally, it is possible to set a criterion for the Fresnel phase term to be considered. A practical criterion will be to consider this effect when the Fresnel phase term $\frac{kr''^2}{2r}[1 - (\hat{s}'' \cdot \hat{r}'')^2]$ is larger than F where the value F is arbitrarily set. In the problem of Fresnel diffraction discussed in [12], the Fresnel effect is considered when $z < a^2/\lambda$ (or $\frac{ka^2}{2z} > \pi$), where a is the size of the aperture and z is the distance from the aperture. In [11], the observation point is considered to be in the Fresnel zone of the aperture diffraction when $r < 2D^2/\lambda$ (or $\frac{ka^2}{2r} > \frac{\pi}{8}$) where r is the distance from the aperture and $D = 2a$ is the aperture diameter. In this study, it is chosen that the Fresnel zone effect be considered when $\frac{kr''^2}{2r} > \frac{\pi}{8}$, which is the stricter criterion of the two criteria discussed here.

For the amplitude correction, only the first order correction term from the far field approximation is considered. Referring to Figure 1, in the far field approximation, it is assumed that the distance $|\bar{r} - \bar{r}''| \approx r$. However, when the observation point C is close to the scatterer, $|\bar{r} - \bar{r}''|$ (or BC) can be approximated by AC which is given as $r - OB \cos \vartheta$. Thus, $|\bar{r} - \bar{r}''| \approx r - OB \cos \vartheta \approx r - \hat{s}'' \cdot \bar{r}''$ where \bar{r}'' is the vector \overline{OB} and \hat{s}'' is the unit vector in the direction of OA . Thus, the amplitude correction in (7) considers the difference between the distance OC and BC . It is also expected that the amplitude correction is larger at small ϑ than at large ϑ .

2.2 Scattered Fields of Disk-shaped and Needle-shaped Scatterers

By substituting the approximation terms in (6) and (7) and the internal field of the ellipsoidal scatterers specialized to disks and needles

into the scattered field expression in (4), we have [10]

$$\begin{aligned}
 \hat{p}_{sl} \cdot \overline{E}_{sl}(\vec{r}) &= \frac{\exp(-jkr)}{r} \hat{p}_{sl} \cdot \frac{k^2(\epsilon_r - 1)}{4\pi} \overline{a}_{shape} \cdot \hat{q}_{il} E_{Oq} \int_{V''} \left[1 + \frac{\hat{s}'' \cdot \vec{r}''}{r} \right] \\
 &\quad \exp \left\{ j\vec{q}'' \cdot \vec{r}'' - j \frac{kr''^2}{2r} [1 - (\hat{s}'' \cdot \hat{r}'')^2] \right\} d\vec{r}'' \\
 &= \left\{ \hat{p}_{sl} \cdot \left[\frac{k^2(\epsilon_r - 1)}{4\pi} \overline{a}_{shape} I_{shape} \right] \right\} \cdot \hat{q}_{il} E_{Oq} \frac{\exp(-jkr)}{r} \\
 &= \hat{p}_{sl} \cdot \overline{f}_{pql}(\overline{k}_s, \overline{k}_i) \cdot \hat{q}_{il} E_{Oq} \frac{\exp(-jkr)}{r} \tag{13}
 \end{aligned}$$

where $\overline{f}_{pql}(\overline{k}_s, \overline{k}_i)$ is the scattering amplitude matrix in the local frame with local incident \hat{q}_{il} polarization and scattered \hat{p}_{sl} polarization and $\overline{k}_s, \overline{k}_i$ are the scattering and incident propagation unit vectors, respectively. \overline{a} is the polarizability tensor defined in [4]. The subscript *shape* refers to either disk or needle and

$$\begin{aligned}
 I_{shape} &= \int_{V''} \left[1 + \frac{\hat{s}'' \cdot \vec{r}''}{r} \right] \exp \left\{ j\vec{q}'' \cdot \vec{r}'' - j \frac{kr''^2}{2r} [1 - \hat{s}'' \cdot \hat{r}'')^2] \right\} d\vec{r}'' \\
 \vec{q}'' &= k(\hat{s}'' - \hat{i}'') = \hat{x}'' q''_x + \hat{y}'' q''_y + \hat{z}'' q''_z, \quad \hat{s}'' = \hat{x}'' s''_x + \hat{y}'' s''_y + \hat{z}'' s''_z \tag{14}
 \end{aligned}$$

where

$$\begin{aligned}
 s''_x &= \sin \theta_{sl} \cos \phi_{sl}, \quad s''_y = \sin \theta_{sl} \sin \phi_{sl}, \quad s''_z = \cos \theta_{sl} \\
 q''_x &= k(s''_x - \sin \theta_{il} \cos \phi_{il}), \quad q''_y = k(s''_y - \sin \theta_{il} \sin \phi_{il}), \tag{15} \\
 q''_z &= k(s''_z - \cos \theta_{il})
 \end{aligned}$$

For the scattering amplitude of the scatterer (either disk or needle) with the incorporation of the amplitude and the Fresnel phase corrections, the expression of I_{shape} is as given in (14). The amplitude correction is included by considering the term $\frac{\hat{s}'' \cdot \vec{r}''}{r}$ in (14) and the Fresnel phase correction is taken into account by considering the term $\exp\{-j \frac{kr''^2}{2r} [1 - (\hat{s}'' \cdot \hat{r}'')^2]\}$ in (14). For far field approximation (or the case where no correction is considered), both the terms ($\frac{\hat{s}'' \cdot \vec{r}''}{r}$ and $\exp\{-j \frac{kr''^2}{2r} [1 - (\hat{s}'' \cdot \hat{r}'')^2]\}$) in (14) will not be considered.

Detailed expressions of I_{disk} and I_{needle} are included in the appendix.

2.3 Scattered Fields of Cylindrical Scatterers

In the derivation of scattered field of a finite length dielectric cylinder (radius = a , length = L), the internal field in the cylinder is obtained through the infinite cylinder approximation. Consider a locally incident plane wave with amplitude vector $\hat{q}_{il}E_{oq}$ and propagation direction specified by θ_{il} and ϕ_{il} in the local frame defined by (ρ'', ϕ'', z'') . The axis of the infinite dielectric cylinder is in the direction of \hat{z}'' . From [6, 7], the internal field of the cylinder due to this plane wave is given by (also [8, 10])

$$\bar{E}_{int} = (\hat{x}''E_{xq} + \hat{y}''E_{yq} + \hat{z}''E_{zq})(\hat{q}_{il} \cdot \hat{q}_{il}E_{oq}) \quad (16)$$

where

$$\begin{aligned} E_{xq} &= \sum_{n=-\infty}^{\infty} \left\{ c_{nq}J_{n+1}(\lambda_i\rho'') \exp(j\phi'') + \right. \\ &\quad \left. d_{nq}J_{n-1}(\lambda_i\rho'') \exp(-j\phi'') \right\} F_n \\ &= E_{oxq} \exp(-jkz'' \cos \theta_{il}) \\ E_{yq} &= -j \sum_{n=-\infty}^{\infty} \left\{ c_{nq}J_{n+1}(\lambda_i\rho'') \exp(j\phi'') - \right. \\ &\quad \left. d_{nq}J_{n-1}(\lambda_i\rho'') \exp(-j\phi'') \right\} F_n \\ &= E_{oyq} \exp(-jkz'' \cos \theta_{il}) \\ E_{zq} &= \sum_{n=-\infty}^{\infty} e_{nq}J_n(\lambda_i\rho'') F_n \\ &= E_{ozq} \exp(-jkz'' \cos \theta_{il}) \end{aligned} \quad (17)$$

where $J_n()$ is the Bessel function and \hat{q}_{il} can be \hat{v}_{il} or \hat{h}_{il} . The common term $\exp(-jkz'' \cos \theta_{il})$ in E_{xq} , E_{yq} , E_{zq} is factored out from F_n . The other expressions are

$$\begin{aligned}
F_n &= j^{-n} \exp[jn(\phi'' - \phi_{il}) - jkz'' \cos \phi_{il}] \\
\lambda_i &= k(\varepsilon_r - \cos^2 \theta_{il})^{\frac{1}{2}} \\
c_{nq} &= 0.5k(\eta h_{nq} + j e_{nq} \cos \theta_{il}) / \lambda_i \\
d_{nq} &= 0.5k(\eta h_{nq} - j e_{nq} \cos \theta_{il}) / \lambda_i \\
e_{nv} &= \frac{j \sin \theta_{il}}{J_n(u) R_n} \left[\frac{H_n^{(2)'}(w)}{w H_n^{(2)}(w)} - \frac{\mu_r J_n'(u)}{u J_n(u)} \right] \\
h_{nv} &= \frac{n \cos \theta_{il} \sin \theta_{il}}{\eta J_n(u) R_n} \left[\frac{1}{w^2} - \frac{1}{u^2} \right] \\
R_n &= \frac{\pi w^2}{2} H_n^{(2)}(w) \left\{ \left[\frac{H_n^{(2)'}(w)}{w H_n^{(2)}(w)} - \frac{\varepsilon_r J_n'(u)}{u J_n(u)} \right] \right. \\
&\quad \left. \left[\frac{H_n^{(2)'}(w)}{w H_n^{(2)}(w)} - \frac{\mu_r J_n'(u)}{u J_n(u)} \right] - n^2 \cos^2 \theta_{il} \left(\frac{1}{w^2} - \frac{1}{u^2} \right)^2 \right\} \\
e_{nh} &= \frac{n \cos \theta_{il} \sin \theta_{il}}{J_n(u) R_n} \left[\frac{1}{w^2} - \frac{1}{u^2} \right] \\
h_{nv} &= \frac{-j \sin \theta_{il}}{\eta J_n(u) R_n} \left[\frac{H_n^{(2)'}(w)}{w H_n^{(2)}(w)} - \frac{\varepsilon_r J_n'(u)}{u J_n(u)} \right] \\
&\text{and } u = \lambda_i a, \quad w = \lambda a, \quad \lambda = k \sin \theta_{il}.
\end{aligned} \tag{18}$$

In the above equations, $H_n^{(2)}(\cdot)$ is the Hankel function of the second kind; $H_n^{(2)'}$ and J_n' are the derivatives with respect to the argument. η is the intrinsic impedance of the free space; ε_r and μ_r are the relative permittivity and permeability of the cylinder.

After substituting the internal field of the cylinder into the scattered field expression in (4) and taking into consideration the Fresnel phase correction terms and amplitude correction terms, the scattered field from the cylinder in the local frame is given by

$$\begin{aligned}
 \hat{p}_{sl} \cdot \bar{E}_{sl}(\bar{r}) &= \frac{k^2(\varepsilon_r - 1)}{4\pi} \int_{V''} \frac{\exp(-jk|\bar{r} - \bar{r}''|)}{|\bar{r} - \bar{r}''|} (\hat{p}_{sl} \cdot \bar{E}_{\text{int}}) d\bar{r}'' \\
 &= \frac{\exp(-jkr)}{r} \hat{p}_{sl} \cdot \frac{k^2(\varepsilon_r - 1)}{4\pi} \\
 &\quad \int_{V''} (\hat{x}'' E_{xq} + \hat{y}'' E_{yq} + \hat{z}'' E_{zq}) \hat{q}_{il} \cdot \hat{q}_{il} E_{oq} \cdot \left[1 + \frac{(\hat{s}'' \cdot \bar{r}'')}{r} \right] \\
 &\quad \exp \left\{ j\bar{q}'' \cdot \bar{r}'' - j \frac{kr''^2}{2r} [1 - (\hat{s}'' \cdot \hat{r}'')^2] \right\} d\bar{r}'' \\
 &= \left\{ \hat{p}_{sl} \cdot \left[\frac{k^2(\varepsilon_r - 1)}{4\pi} \bar{I}_c \hat{q}_{il} \right] \right\} \cdot \hat{q}_{il} E_{oq} \frac{\exp(-jkr)}{r} \\
 &= \hat{p}_{sl} \cdot \bar{f}_{pq}(\bar{k}_s, \bar{k}_i) \cdot \hat{q}_{il} E_{oq} \frac{\exp(-jkr)}{r}
 \end{aligned} \tag{19}$$

The integration vector \bar{I}_c in (19) which includes the Fresnel phase correction term ($\exp \left\{ -j \frac{kr''^2}{2r} [1 - (\hat{s}'' \cdot \hat{r}'')^2] \right\}$) and the amplitude correction ($\frac{(\hat{s}'' \cdot \bar{r}'')}{r}$) term is given by

$$\begin{aligned}
 \bar{I}_c &= \int_v \left(1 + \frac{\hat{s}'' \cdot \bar{r}''}{r} \right) \bar{E}_q \\
 &\quad \exp \left(jk(\hat{s}'' \cdot \bar{r}'') - j \frac{kr''^2}{2r} [1 - (\hat{s}'' \cdot \hat{r}'')^2] - jkz'' \cos \theta_{il} \right) d\bar{r}'' \tag{20}
 \end{aligned}$$

where $\bar{E}_q = \hat{x}'' E_{oxq} + \hat{y}'' E_{oyq} + \hat{z}'' E_{ozq}$. For far field approximation (no correction case), both the Fresnel phase and the amplitude correction terms are not included.

In the local frame cylindrical coordinate system, (20) can be written as

$$\begin{aligned}
 \bar{I}_c &= \int_v \left(1 + \frac{s''_x \rho'' \cos \phi'' + s''_y \rho'' \sin \phi'' + s''_z z''}{r} \right) \bar{E}_q \\
 &\quad \cdot \exp \left\{ jk(s''_x \rho'' \cos \phi'' + s''_y \rho'' \sin \phi'' + s''_z z'') \right. \\
 &\quad \left. - j \frac{k(\rho''^2 + z''^2)}{2r} \left[1 - \frac{(s''_x \rho'' \cos \phi'' + s''_y \rho'' \sin \phi'' + s''_z z'')^2}{\rho''^2 + z''^2} \right] \right. \\
 &\quad \left. - jkz'' \cos \theta_{il} \right\} d\bar{r}'' \tag{21}
 \end{aligned}$$

where the following expressions have been used:

$$\begin{aligned}
 \bar{r}'' &= \rho'' \cos \phi'' \hat{x}'' + \rho'' \sin \phi'' \hat{y}'' + z'' \hat{z}'', \\
 \hat{r}'' &= \frac{\rho'' \cos \phi'' \hat{x}'' + \rho'' \sin \phi'' \hat{y}'' + z'' \hat{z}''}{\sqrt{\rho''^2 + z''^2}} \\
 r''^2 &= \rho''^2 + z''^2, \quad \hat{s}'' = s_x'' \hat{x}'' + s_y'' \hat{y}'' + s_z'' \hat{z}'' \\
 \hat{s}'' \cdot \bar{r}'' &= s_x'' \rho'' \cos \phi'' + s_y'' \rho'' \sin \phi'' + s_z'' z'', \\
 \hat{s}'' \cdot \hat{r}'' &= \frac{s_x'' \rho'' \cos \phi'' + s_y'' \rho'' \sin \phi'' + s_z'' z''}{\sqrt{\rho''^2 + z''^2}}
 \end{aligned} \tag{22}$$

In order to simplify the expressions in (21), the following assumptions are made:

Assumption 1: As the internal field is obtained through the infinite cylinder approximation, we assume that $L/2 \gg a$, where L and a are the length and the radius of the cylinder, respectively.

Assumption 2: It is assumed that the term $\frac{k\rho''^2}{2r}$ in (21) is small and can be neglected. Since the term $\frac{k\rho''^2}{2r}$ is a phase term, in order for this assumption to be valid, it requires that $\frac{k\rho''^2}{2r} < \frac{\pi}{8}$ where the value $\frac{\pi}{8}$ is chosen arbitrarily [11]. From Assumption 1, the term $\frac{kz''^2}{2r}$ is generally larger than the term $\frac{k\rho''^2}{2r}$ by a factor of $\frac{z''^2}{\rho''^2}$.

Assumption 3: It is assumed that the integration contributions from the z'' term in $\left(1 + \frac{s_x'' \rho'' \cos \phi'' + s_y'' \rho'' \sin \phi'' + s_z'' z''}{r}\right)$ (referred to as Term A) and $j \frac{k(\rho''^2 + z''^2)}{2r} \left[1 - \frac{(s_x'' \rho'' \cos \phi'' + s_y'' \rho'' \sin \phi'' + s_z'' z'')^2}{\rho''^2 + z''^2}\right]$ (referred to as Term B) are generally larger than those from the ρ'' term. For cases when $z'' > \rho''$, this is generally true as Assumption 1 requires $L/2 \gg a$ and r is either larger or of the same order as $L/2$ (for application in a dense medium, r is taken to be the average distance between the scatterers). For cases when $\rho'' > z''$, the ρ'' term in Term A is small compared with r and from Assumption 2, Term B can be ignored.

Thus, after considering these three assumptions, (21) can be reduced and arranged to be

$$\begin{aligned}
 \bar{I}_c &= \int_v \left(1 + \frac{s_z'' z''}{r}\right) \bar{E}_q \cdot \exp\left\{j\lambda_s \rho'' \cos(\phi'' - \phi_{sl}) - \right. \\
 &\quad \left. j \frac{kz''^2}{2r} [1 - s_z''^2] + jkz''(s_z'' - \cos \theta_{il})\right\} d\bar{r}'' \tag{23}
 \end{aligned}$$

where $\lambda_s = k\sqrt{(s_x''^2 + s_y''^2)} = k \sin \theta_{sl}$ and ϕ_{sl} is the arc tangent of s_y''/s_x'' .

Since \overline{E}_q contains terms in ϕ'' and ρ'' (such as $e^{j(n\pm 1)\phi''}$ and $J_{n\pm 1}(\lambda_i \rho'')$), the integration in (23) should include the ϕ'' and the ρ'' terms in \overline{E}_q . By collecting all the terms with ϕ'' , the integration of ϕ'' can then be written in the following form,

$$I_{o\phi}(n \pm 1) = \int_0^{2\pi} \exp[j(n \pm 1)\phi''] \exp[j\lambda_s \rho'' \cos(\phi'' - \phi_{sl})] d\phi'' \quad (24)$$

Expanding the exponential function into Bessel functions with the following relation [13]:

$$\exp[-j\beta\rho \cos \phi] = \sum_{m=-\infty}^{\infty} j^{-m} J_m(\beta\rho) \exp(jm\phi) \quad (25)$$

Integration in (24) is then given by [8]

$$\begin{aligned} I_{o\phi}(n \pm 1) &= \sum_{m=-\infty}^{\infty} \int_0^{2\pi} \exp[j(n \pm 1)\phi''] j^m J_m(\lambda_s \rho'') \\ &\quad \exp[-jm(\phi'' - \phi_{sl})] d\phi'' \\ &= 2\pi j^{n\pm 1} J_{n\pm 1}(\lambda_s \rho'') \exp[j(n \pm 1)\phi_{sl}] \\ &= I_{\phi}(n \pm 1) I_{n\pm 1}(\lambda_s \rho'') \end{aligned} \quad (26)$$

when $n = n \pm 1$. For other values of m , $I_{o\phi}(n \pm 1)$ is equal to zero. The term that contains ρ'' in (26) will later be integrated with other ρ'' terms in (23).

The integration in ρ'' is given by

$$\begin{aligned} I_{\rho}(n) &= \int_0^a J_n(\lambda_i \rho'') J_n(\lambda_s \rho'') \rho'' d\rho'' \\ &= \frac{a}{\lambda_i^2 - \lambda_s^2} [\lambda_i J_n(\lambda_s a) J_{n+1}(\lambda_i a) - \lambda_s J_n(\lambda_i a) J_{n+1}(\lambda_s a)] \end{aligned} \quad (27)$$

When the radius a (or ρ'') is very small, the combination of (24) and (27) approaches πa^2 which is the case for needle (see Appendix).

From (23), the integration of z'' is given by

$$\begin{aligned} I_z &= \int_{-L/2}^{L/2} \left(1 + \frac{s_z'' z''}{r} \right) \exp \left(jkz''(s_z'' - \cos \theta_{il}) - j \frac{kz''^2}{2r} (1 - s_z''^2) \right) dz'' \\ &= I_{z1} + I_{z2} \end{aligned} \quad (28)$$

where

$$\begin{aligned}
 I_{z1} &= \int_{-L/2}^{L/2} \exp \left(jkz''(s_z'' - \cos \theta_{il}) - j\frac{kz''^2}{2r}(1 - s_z''^2) \right) dz'' \\
 &= \int_{-L/2}^{L/2} \exp \left(jz''q_z'' - j\frac{m_n z''^2}{2} \right) dz'' \\
 I_{z2} &= \int_{-L/2}^{L/2} \frac{s_z'' z''}{r} \exp \left(jkz''(s_z'' - \cos \theta_{il}) - j\frac{kz''^2}{2r}(1 - s_z''^2) \right) dz'' \\
 &= \frac{s_z''}{r} \int_{-L/2}^{L/2} z'' \exp \left(jz''q_z'' - j\frac{m_n z''^2}{2} \right) dz''
 \end{aligned}
 \tag{29}$$

where $q_z'' = k(s_z'' - \cos \theta_{il})$ and $m_n = \frac{k}{r}(1 - s_z''^2)$.

The integration in (29) can be obtained through the same method applied to the needle case (see Appendix) and the final expressions of I_{z1} and I_{z2} in (29) are as follows

$$\begin{aligned}
 I_{z1} &= \exp \left(\frac{j q_z''^2}{2m_n} \right) \sqrt{\frac{\pi}{m_n}} \left\{ f_c(b_1) + f_c(b_2) - j[f_s(b_1) + f_s(b_2)] \right\} \\
 I_{z2} &= \frac{s_z'' q_z''}{r m_n} I_{z1} + \frac{j s_z''}{r m_n} \left[\exp \left(\frac{m_n L^2}{8j} - \frac{L q_z''}{2j} \right) - \exp \left(\frac{m_n L^2}{8j} + \frac{L q_z''}{2j} \right) \right]
 \end{aligned}
 \tag{30}$$

where $b_1 = \sqrt{\frac{m_n}{2}} \left(\frac{L}{2} - \frac{q_z''}{m_n} \right)$, $b_2 = \sqrt{\frac{m_n}{2}} \left(\frac{L}{2} + \frac{q_z''}{m_n} \right)$, $f_c(x)$ and $f_s(x)$ are the Fresnel cosine and sine integral functions.

Combining the results from (26), (27) and (28), the components of \bar{I}_c in (23) are given by

$$\begin{aligned}
 I_{cx} &= \sum_{n=-\infty}^{\infty} e^{-jn\phi_{ii}} \{ c_{nq} I_\phi(n+1) I_\rho(n+1) + d_{nq} I_\phi(n-1) I_\rho(n-1) \} Z \\
 I_{cy} &= \sum_{n=-\infty}^{\infty} e^{-jn\phi_{ii}} \{ d_{nq} I_\phi(n-1) I_\rho(n-1) - c_{nq} I_\phi(n+1) I_\rho(n+1) \} Z \\
 I_{cz} &= \sum_{n=-\infty}^{\infty} e^{-jn\phi_{ii}} \{ e_{nq} I_\phi(n) I_\rho(n) \} Z
 \end{aligned}
 \tag{31}$$

where $Z = j^{-n} I_z$.

The scattering amplitude component in $\bar{f}_{pql}(\bar{k}_s, \bar{k}_i)$ in (19) is then given by

$$f_{pql}(\bar{k}_s, \bar{k}_i) = \frac{k^2(\varepsilon_r - 1)}{4\pi} \sum_{n=-\infty}^{\infty} e^{-jn\phi_{il}} \{ d_{nq} I_\phi(n-1) I_\rho(n-1) \\ (\hat{p}_{sl} \cdot \hat{x}'' + j\hat{p}_{sl} \cdot \hat{y}'') Z + c_{nq} I_\phi(n+1) I_\rho(n+1) \\ (\hat{p}_{sl} \cdot \hat{x}'' - j\hat{p}_{sl} \cdot \hat{y}'') Z + e_{nq} Z I_\phi(n) I_\rho(n) (\hat{p}_{sl} \cdot \hat{z}'') \} \quad (32)$$

Knowing that $Z = j^{-n} I_z$ and $I_\phi(n) = 2\pi j^n e^{jn\phi_{sl}}$, and let $I_z = L\mu_f$, $I_\rho(n) = Z_n$, $A_n = \frac{k}{2\lambda_i}(Z_{n-1} - Z_{n+1})$, $B_n = \frac{k}{2\lambda_i}(Z_{n-1} + Z_{n+1})$ and $C = \frac{k^2 L}{2} \mu_f (\varepsilon_r - 1)$, and use the substitutions below:

$$p = v, h; \quad \hat{v}_{sl} = \cos \theta_{sl} (\cos \phi_{sl} \hat{x}'' + \sin \phi_{sl} \hat{y}'') - \sin \theta_{sl} \hat{z}'', \\ \hat{h}_{sl} = -\sin \phi_{sl} \hat{x}'' + \cos \phi_{sl} \hat{y}'', \\ j\hat{v}_{sl} \cdot \hat{x}'' - \hat{v}_{sl} \cdot \hat{y}'' = j \cos \theta_{sl} \cos \phi_{sl} - \cos \theta_{sl} \sin \phi_{sl} = j \cos \theta_{sl} e^{j\phi_{sl}} \\ j\hat{v}_{sl} \cdot \hat{x}'' + \hat{v}_{sl} \cdot \hat{y}'' = j \cos \theta_{sl} \cos \phi_{sl} + \cos \theta_{sl} \sin \phi_{sl} = j \cos \theta_{sl} e^{-j\phi_{sl}} \\ \hat{v}_{sl} \cdot \hat{z}'' = -\sin \theta_{sl} \\ j\hat{h}_{sl} \cdot \hat{x}'' + \hat{h}_{sl} \cdot \hat{y}'' = -j \sin \phi_{sl} + \cos \phi_{sl} = e^{-j\phi_{sl}} \\ j\hat{h}_{sl} \cdot \hat{x}'' - \hat{h}_{sl} \cdot \hat{y}'' = -j \sin \phi_{sl} - \cos \phi_{sl} = -e^{-j\phi_{sl}} \\ \hat{h}_{sl} \cdot \hat{z}'' = 0 \quad (33)$$

the local frame scattering amplitudes are obtained and have the expressions as shown below:

$$f_{vvl} = C \{ e_{ov} \cos \theta_{il} B_o \cos \theta_{sl} - e_{ov} Z_o \sin \theta_{sl} + 2 \sum_{n=1}^{\infty} [(e_{nv} \cos \theta_{il} B_n - \\ j\eta h_{nv} A_n) \cos \theta_{sl} - e_{nv} Z_n \sin \theta_{sl}] \cos[n(\phi_{sl} - \phi_{il})] \} \\ f_{hhl} = C \{ \eta h_{oh} B_o + 2 \sum_{n=1}^{\infty} (\eta h_{nh} B_n + j e_{nh} \cos \theta_{il} A_n) \cos[n\phi_{sl} - \phi_{il}] \} \\ f_{vhl} = 2jC \sum_{n=1}^{\infty} \{ (e_{nh} \cos \theta_{il} B_n - j\eta h_{nh} A_n) \cos \theta_{sl} - \\ e_{nh} Z_n \sin \theta_{sl} \} \cos[n(\phi_{sl} - \phi_{il})] \\ f_{hvl} = 2jC \sum_{n=1}^{\infty} (\eta h_{nv} B_n + j e_{nv} \cos \theta_{il} A_n) \sin[n(\phi_{sl} - \phi_{il})] \quad (34)$$

3. THEORETICAL ANALYSIS

For the theoretical analysis, the quantity of interest is the backscattering cross section for linear polarization which is defined by [4]

$$\text{Backscattering cross section} = 4\pi \left| f_{pql}(-\hat{i}, \hat{i}) \right|^2 \quad (35)$$

where f_{pql} is the scattering amplitude of the scatterer. \hat{i} is the incident direction and \hat{s} is the scattered direction. For circular polarization, the backscattering cross section is defined by [4, 14]

$$\text{Backscattering cross section} = \pi \left| f_{vvl}(-\hat{i}, \hat{i}) \pm f_{hhl}(-\hat{i}, \hat{i}) \right|^2 \quad (36)$$

where the + and - signs refer to the left-hand (LHC) and right-hand (RHC) circular polarization, respectively.

In order to study the effects of the Fresnel phase correction and the amplitude correction, theoretical analysis which involves comparisons between the scattering cross sections of the scatterers with and without correction for different frequencies and angles are carried out. For the convenience of reference, the case for scattering cross section with no correction added to the scattering amplitude is referred as NCT (No Correction Term). FCT (Fresnel phase Correction Term) refers to the scattering cross section with Fresnel phase correction added to the scattering amplitude and AFCT (Amplitude and Fresnel phase Correction Term) is for the scattering cross section with both amplitude correction and Fresnel phase correction. For the purpose of the analysis carried out in this section, a practical approach is to consider the scattering cross section at a distance d from the scatterer where various values of d can be chosen for the study of the near field effects. It is known that the Fresnel phase correction is related to $\frac{kr''^2}{2d} [1 - (\hat{s}'' \cdot \hat{r}'')^2]$ and the amplitude correction term is proportional to $\frac{\hat{s}'' \cdot \hat{r}''}{d}$ (or $\frac{r''(\hat{s}'' \cdot \hat{r}'')}{d}$). Thus, the distance d is a general parameter for the study of the effects of these two types of corrections.

The scattering geometry used in the following discussions is shown in Figure 2 where a general vector \bar{A} is specified by a polar angle θ and an azimuthal angle ϕ .

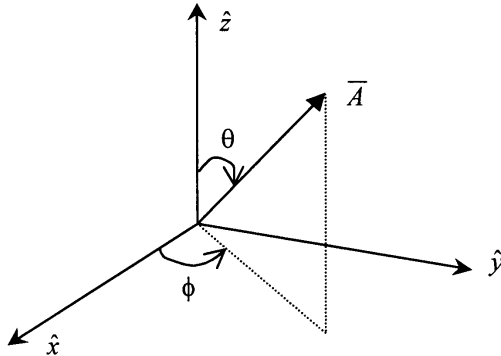


Figure 2. Geometry of the scattering problem.

3.1 Disk

Consider a disk placed in the geometry system shown in Figure 2 where the axis of the disk is parallel to the z -axis and the surface of the disk is on the x - y plane. The dimensions of the disk are chosen to be $a = b = 5$ cm and $c = 0.1$ mm and the relative permittivity of the disk is $\epsilon_r = 15 - j5$. The background medium is free space. The distance of the observation point from the centre of the scatterer d is chosen to be 10 cm.

Figure 3 shows the effects of the phase and the amplitude corrections to the VV backscattering cross section at 20° incident angle (20° from the $+\hat{z}$ axis) for different values of ka where k is the wavenumber in free space. The upper x -axis scale shows the corresponding values of $\frac{ka^2}{2d}$. For ease of reference, $\frac{ka^2}{2d}$ is referred as the Fresnel factor. From Figure 3, it is noticed that the Fresnel phase correction is not important until the Fresnel factor $\frac{ka^2}{2d}$ is larger than 0.9 ($ka \gtrsim 3.6$). The effect of amplitude correction is also observed in this region ($ka \gtrsim 3.6$) by comparing the theoretical results of FCT and that of AFCT. It should be noted that the magnitude of the amplitude correction term is related to $\frac{r''(\hat{s}'' \cdot \hat{r}'')}{d}$. Generally, the integration of the amplitude correction term alone ($\frac{r''(\hat{s}'' \cdot \hat{r}'')}{d}$) over the volume of the disk is small compared with unity because the thickness of the disk is much smaller than the distance d . However, when it is integrated together with the phase term (which also includes the Fresnel phase correction term) as in (14), the interaction between the amplitude correction term and the phase term may cause the overall contribution to

be different from the contribution from the phase term alone. Thus, for the region $ka \lesssim 3.6$ (or $kc \lesssim 0.0072$) where the contribution from the variation in phase term for the volume elements in the disk is small (close to Rayleigh scattering region) or negligible (in the Rayleigh scattering region), the effect of the amplitude correction is very small and can be neglected. However, when ka increases further ($ka \gtrsim 3.6$), the contribution from the variation in phase term for the volume elements in the disk is important, especially when the Fresnel phase correction term becomes significant, thus the effect of the amplitude correction becomes noticeable. It should be noted that for far field approximation where d is assumed to be large, this effect of the amplitude correction is negligible. For the region ($ka \gtrsim 3.6$) where both the Fresnel phase correction and the amplitude correction are important, the effect of amplitude correction is found to be smaller compared with that of the Fresnel phase correction. This is because the incident angle is 20° and near to the surface normal of the disk, and the angle ϑ ($\cos \vartheta = \hat{s}'' \cdot \hat{r}''$) discussed in Section 2 of this paper is generally large (close to 90°) for most of the volume elements in the disk at this incident angle. In the expression for angle ϑ , \hat{s}'' is the local frame scattering unit vector and \hat{r}'' is the location unit vector to volume elements of the disk in the local frame. Since the Fresnel phase correction is related to $\frac{kr''^2}{2d}[1 - (\hat{s}'' \cdot \hat{r}'')^2]$ and the amplitude correction is proportional to $\frac{r''(\hat{s}'' \cdot \hat{r}'')}{d}$, a large value of angle ϑ (close to 90°) means that the Fresnel phase correction is more important than the amplitude correction. It should also be noted that direct comparison of the two terms is difficult as the Fresnel phase correction is a phase term and related to kr''^2 and the amplitude correction term is an amplitude term and related to r'' .

Figure 4 shows the plot for HH backscattering cross section. As the incident angle is close to the normal incidence to the surface of the disk, there is not much difference between the plots of VV and HH and the same trend of the effects of the various corrections is also observed in Figure 4.

It would be interesting to study the angular behavior of the backscattering cross sections from various theories at high frequency. Figures 5 and 6 show the VV backscattering cross sections of the same disk at 9.6 GHz where the Fresnel phase correction and the amplitude correction are important. In Figure 5, FCT cases for various values of d (10 cm, 26 cm and 46 cm) are plotted together with the NCT

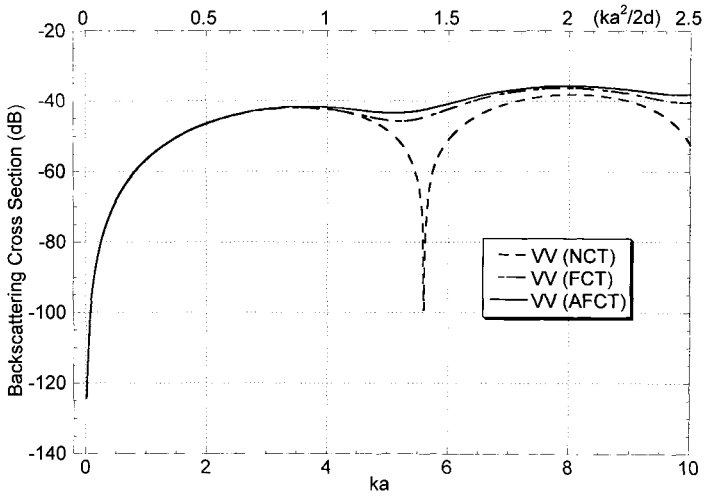


Figure 3. Comparison between theories for VV backscattering cross section for different values of ka at 20° incident angle for a disk with $a = b = 5$ cm and $c = 0.1$ mm .

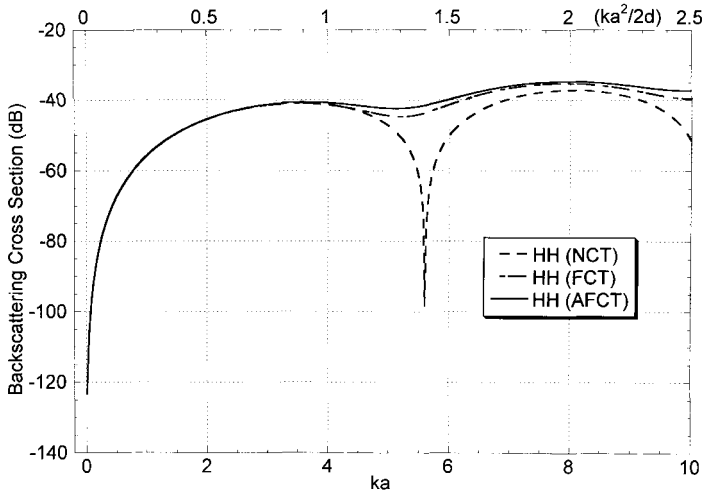


Figure 4. Comparison between theories for HH backscattering cross section for different values of ka at 20° incident angle for a disk with $a = b = 5$ cm and $c = 0.1$ mm .

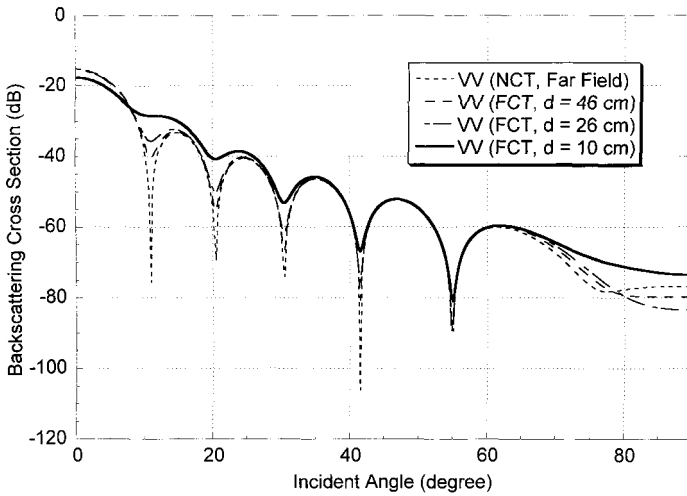


Figure 5. Comparison between theories (NCT and FCT) for VV backscattering cross section for different angles at 9.6 GHz for a disk with $a = b = 5$ cm and $c = 0.1$ mm .

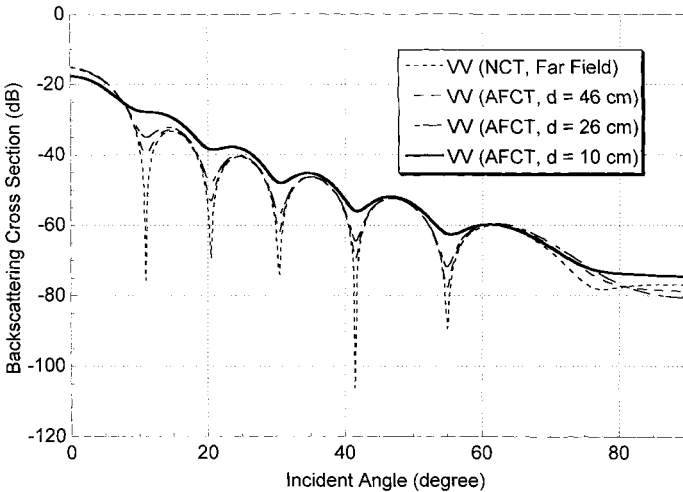


Figure 6. Comparison between theories (NCT and AFCT) for VV backscattering cross section for different angles at 9.6 GHz for a disk with $a = b = 5$ cm and $c = 0.1$ mm .

case. It can be seen that when d is decreased, generally the effect of the Fresnel phase correction becomes larger, especially at the null locations. It should be noted that for small incident angles, the phase term $\exp(j\bar{q}'' \cdot \bar{r}'')$ in equation (14) in backscattering direction is generally small as the angle between $\bar{q}'' = k(\hat{s}'' - \hat{i}'')$ and \bar{r}'' is near to 90° . Thus, the phase contribution is generally contributed by the Fresnel phase correction terms. For large incident angles, both phase contributions are to be considered together and the interaction between these two contributions may account for the variation of the curves for various FCT cases.

In Figure 6, the AFCT cases for VV backscattering cross sections for different values of d ($d = 10$ cm, 26 cm and 46 cm) are plotted. By comparing the corresponding curves in this figure and those of Figure 5 (for example, the FCT and the AFCT cases for $d = 10$ cm), it is found that the effect of amplitude correction is noticeable for incident angles $\gtrsim 30^\circ$. This dependence on the angle has been discussed in Figure 3. The corresponding plots of Figure 5 and Figure 6 for HH case are not included as they show the same trends for various corrections as discussed in the VV case. The major difference is that for the HH polarization case, its backscattering cross sections are higher than those of the VV polarization case at high incident angles and approach to be the same for low incident angle. This is expected because at 0° incident angle, both the VV and the HH cases present a similar scattering problem for a circular disk.

3.2 Needle

Consider now a needle is placed in the geometry shown in Figure 2 where its axis is in the direction of z -axis. The dimensions of the needle selected are $a = b = 0.2$ mm and $h = \frac{2}{3}c = 5$ cm, where h is the half length of the needle. The relative permittivity chosen is $\epsilon_r = 9.6 - j4.03$ and the distance d is fixed at 10 cm.

Figure 7 shows the VV backscattering cross sections of the needle at 20° incident angle (20° from the $+\hat{z}$ axis) for different values of ka (up to $ka = 0.1$). The scale for the Fresnel factor ($\frac{kh^2}{2d}$ in this case) is plotted along the upper x -axis of the graphs. It is generally found that the Fresnel correction is not important at this incident angle as the angle ϑ between the scattered direction and the location vector to the volume elements (in these cases, most of them are in the $\pm z$ direction) is small. As discussed in Figure 3, the small angle of ϑ

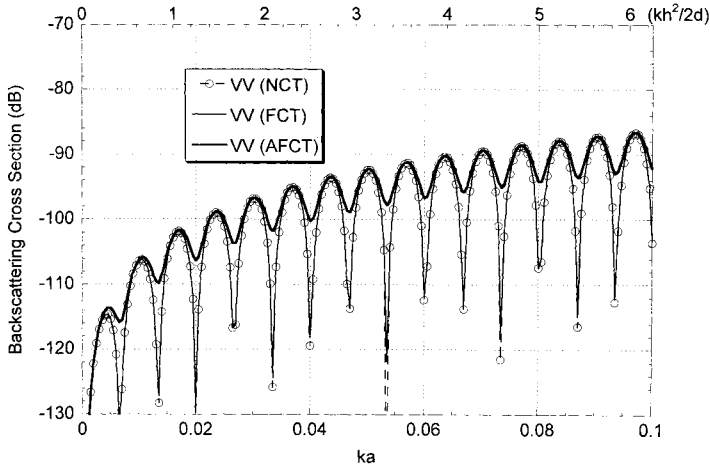


Figure 7. Comparison between theories for VV backscattering cross section for different values of ka at 20° incident angle for a needle with $a = b = 0.2$ mm and $h = 5$ cm.

means that the amplitude correction is important for a close distance d which is of the order of the length of the needle. This correction is needed in the resonance region ($ka \gtrsim 0.0035$) as shown in Figure 7. For Rayleigh scattering region ($ka \lesssim 0.0035$), the effect is negligible.

The effects of corrections for various incident angles for the needle are studied at 9.6 GHz where the amplitude and the Fresnel phase corrections are necessary to be considered and these are observed in Figure 8 and Figure 9 plotted for the VV case. Same observation is obtained for the HH case. In Figure 8, the curves for various FCT cases ($d = 10$ cm, 26 cm and 46 cm) are plotted together with the NCT case for comparison purpose. It is shown that in the case of the needle, the Fresnel phase correction is needed for high incident angles where the angles ϑ are close to 90° . For the amplitude correction, it is shown to be important at low incident angle by comparing the curves for FCT in Figure 8 and the curves for AFCT in Figure 9.

3.3 Cylinder

Referring to the geometry shown in Figure 2 where the axis of the cylinder is aligned in the direction of z -axis. The dimensions of the cylinder are chosen to be $a = 0.2$ cm and $h = \frac{2}{3}c = 5$ cm, where h is the half length of the cylinder. The relative permittivity chosen is

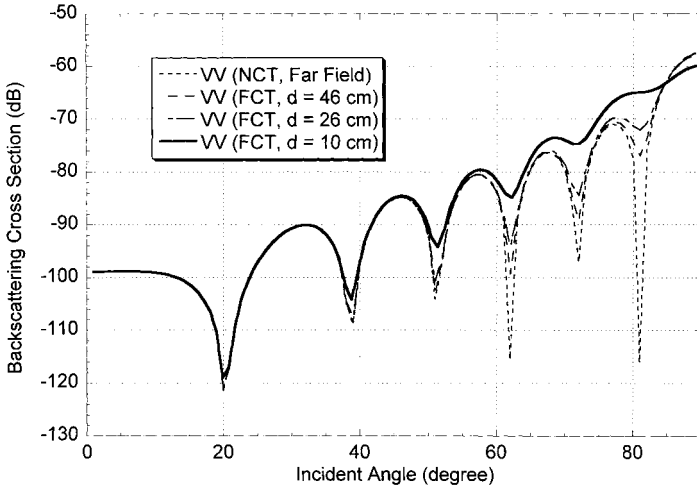


Figure 8. Comparison between theories (NCT and FCT) for VV backscattering cross section for different angles at 9.6 GHz for a needle with $a = b = 0.2$ mm and $h = 5$ cm .

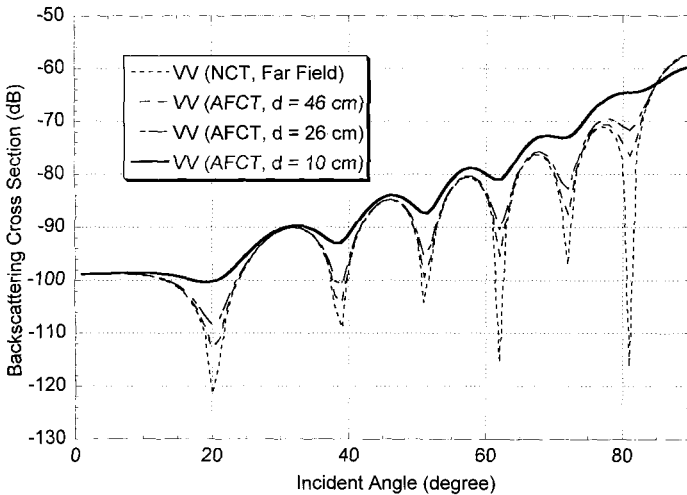


Figure 9. Comparison between theories (NCT and AFCT) for VV backscattering cross section for different angles at 9.6 GHz for a needle with $a = b = 0.2$ mm and $h = 5$ cm .

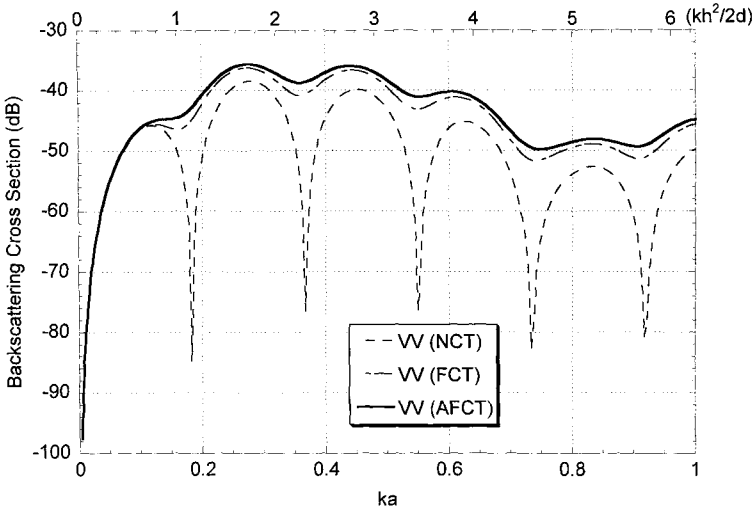


Figure 10. Comparison between theories for VV backscattering cross section for different values of ka at 70° incident angle for a cylinder with $a = b = 0.2$ cm and $h = 5$ cm.

$\varepsilon_r = 9.6 - j4.03$ and the distance d is again fixed at 10 cm. Using the formulation presented in Section 2.3 on cylinder, a study of the backscattering cross sections of the cylinder is carried out.

Basically, it is found that the effects of the amplitude and the Fresnel phase corrections on the backscattering cross sections of the needle and the cylinder at low ka present the same trend as both types of scatterer has the same elongated structures into the two ends. For the cylinder, the case of 70° incident angle (70° from the axis) is included in Figure 10 to show the VV backscattering cross sections plotted against ka ($ka < 1.0$) for the NCT, FCT and AFCT cases. The scale for the Fresnel factor $\frac{kh^2}{2d}$ is also included. For high incident angle of 70° , the effect of the Fresnel phase correction is obvious from Figure 10 for $\frac{kh^2}{2d} \gtrsim 0.8$ and is larger than the effect of the amplitude correction which shows up for $ka \gtrsim 0.11$. The plot for the HH case is not included as the same trend is observed.

Figure 11 shows the effects of Fresnel phase correction and the amplitude correction for various incident angles at 9.6 GHz. In Figure 11, the curves for the VV backscattering cross section for the NCT case, the FCT case ($d = 10$ cm) and the AFCT case ($d = 10$ cm) are plotted. It is clearly shown that the Fresnel phase correction is more

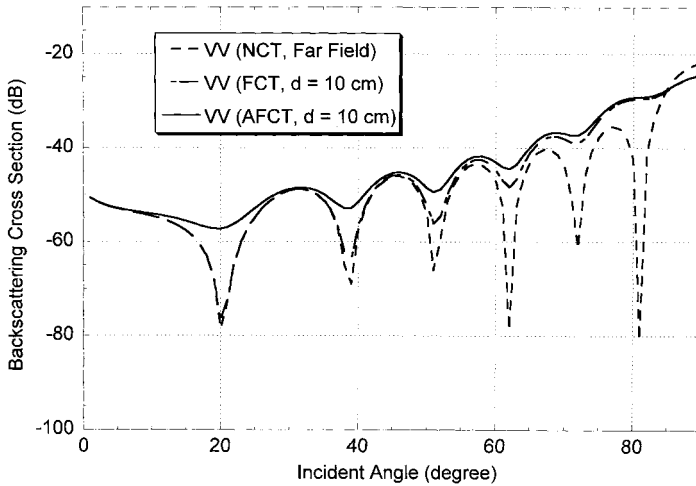


Figure 11. Comparison between theories (NCT, FCT, and AFCT) for VV backscattering cross section for different angles at 9.6 GHz for a cylinder with $a = b = 0.2$ cm and $h = 5$ cm .

important at high incident angle (by comparing the NCT and the FCT curves), as in the case of needle. For the amplitude correction, its effect is observed for low incident angle (by comparing the FCT and the AFCT curves).

4. COMPARISONS WITH MEASUREMENT DATA

A series of measurement on the backscattering cross sections of dielectric bodies was done in [14, 15]. Figures 12 and 13 show the comparisons between the theories (NCT and AFCT) and their measurement results at 2.86175 GHz for circular disk samples and rod samples, respectively. The measurement was done using circular polarization and the normalized backscattering cross sections (σ/λ^2) for right hand circular polarization are plotted against the incident angle in Figures 12 and 13. The expression of the backscattering cross section (σ) for circular polarization is given in (36). For the circular disk case, three samples were selected and denoted as Disk 1, Disk 2 and Disk 3. The parameters of the samples are listed in Table 1 where h is half the thickness of the disk.

Figure 12 shows the comparisons between the measurement data and the theoretical calculations for the NCT and AFCT cases. It is

	Disk 1	Disk 2	Disk 3
a (cm)	1.27	2.54	5.08
ka	0.762	1.523	3.042
h/a	0.1060	0.1	0.1009
ϵ_r	$3.12 - j0.036$	$3.11 - j0.036$	$3.10 - j0.036$

Table 1. Parameters of the disk samples used in [14].

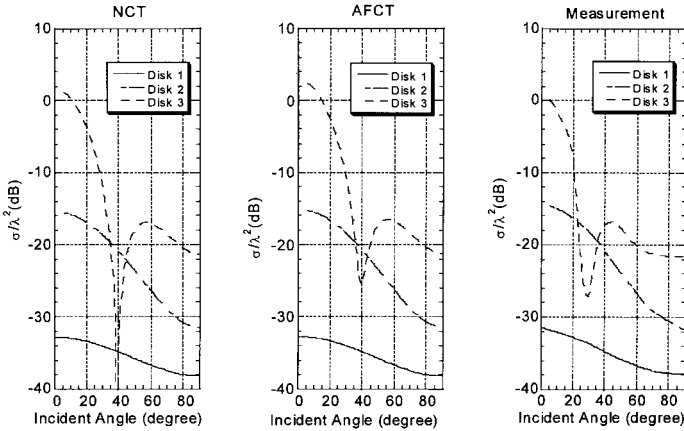


Figure 12. Comparisons between theories and measurement data (Allan & McCormick, 1980) for three disk samples illuminated by a circularly polarized wave.

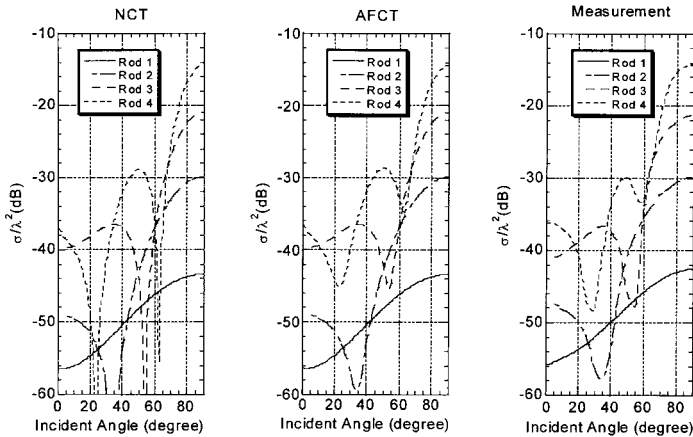


Figure 13. Comparisons between theories and measurement data (Allan & McCormick, 1980) for four rod samples illuminated by a circularly polarized wave.

found that the NCT predictions agree generally in trend and level with the measurement results except at the null locations. For the AFCT case with d fixed at 24 cm, the theoretical results seem to give a good match with the measurement results. For disk 3, there is a slight shift of the null location in Figure 12 to the right as compared with the measurement data, but for disks 1 and 2, there is good agreement between the AFCT predictions and the measurement data.

For the rods, the parameters of the four samples used in the measurement are listed in Table 2. In Figure 13, the measurement data are compared with the theoretical results for the NCT and the AFCT cases. For the four rod samples considered, the NCT calculations again show the same trend and level with the measurement data except at null locations. The AFCT results with $d = 24$ cm give a better match with the measurement data and decrease the difference between the theoretical results and the measurement data at null locations.

	Rod 1	Rod 2	Rod 3	Rod 4
a (mm)	1.91	3.18	4.45	5.72
ka	0.1143	0.1904	0.2666	0.3428
h/a	10.00	9.99	9.99	10.00
ε_r	$3.13 - j0.036$	$3.13 - j0.036$	$3.15 - j0.036$	$3.14 - j0.036$

Table 2. Parameters of the rod samples used in [14].

Comparisons between the theoretical results and the measurement data from an aspen leaf and a birch stick are also carried out. The measurements were acquired by Allan et al. by illuminating the objects with a circularly polarized wave at 9.6 GHz [4]. The physical parameters of the aspen leaf are $a = 2.275$ cm, $h = 0.1$ mm and the leaf gravimetric moisture content (M_g) is chosen as 0.5. Using the permittivity model developed in [16], the relative permittivity is $\varepsilon_r \approx 12.49 - 5.08$. Figure 14 shows the comparisons between the measurement data and the theoretical results (NCT and AFCT). There is good agreement between the measurement data and the NCT calculation at low incident angle where the incident direction is close to the surface normal of the leaf. For other angles, similar trend is generally observed between the NCT calculation and the measurement data except at the null locations where the difference is large. For the AFCT results with d fixed

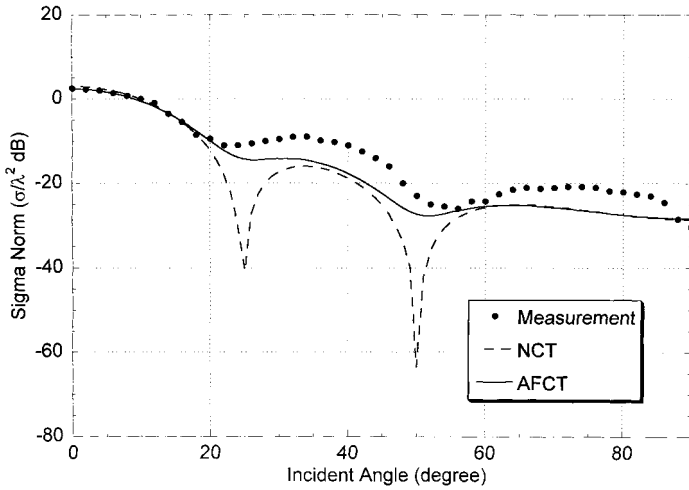


Figure 14. Comparisons between theories and measurement data for an aspen leaf illuminated by a circularly polarized plane wave (Allan et al., 1986).

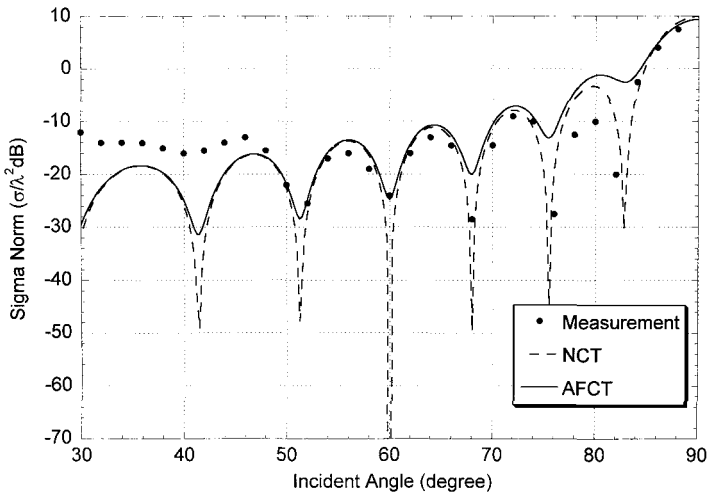


Figure 15. Comparisons between theories and measurement data for a birch stick illuminated by a circularly polarized plane wave (Allan et al., 1986).

at 4 cm, there seems to be a better agreement with the measurement data and the difference at null locations is smaller compared with that of the NCT case.

For the birch stick, the dimensions are $a = 0.95$ cm and $h = 6.25$ cm and the relative permittivity is assumed to be $9.6 - j4.03$. Figure 15 shows the comparisons between the measurement data and the theoretical results (NCT and AFCT). For the NCT case, it is found that there is a good match in trend with the measurement data for high incident angles ($\gtrsim 50^\circ$). However, there is some difference for low incident angles and at null locations. The AFCT case for $d = 32.8$ cm shows some improvement in the matching at some null locations but the difference at low incident angles remains. This difference in level at low incident angles may be due to the edge diffraction effect of the stick as the ends of the stick and the flat ends of the cylinder used in the model may be different.

5. CONCLUSION

In conclusion, it is found from the discussion and results presented in this study that the amplitude and the Fresnel phase corrections are important to be considered in the scattered fields of the disks, needles and cylinders when the Fresnel zone effect needs to be included. Fresnel factor is found to be a good indicator for the need of the amplitude and the Fresnel phase corrections. With the inclusion of the amplitude and the Fresnel phase corrections, good matches between the theoretical results and the measurement data for single scatterer (disk, rod, birch stick and aspen leaf) are obtained.

APPENDIX

For disks, the integral term in (14) can be divided into two parts as shown below:

$$\begin{aligned} I_{disk} &= \int_{V''} \left[1 + \frac{r''}{r} (\hat{s}'' \cdot \hat{r}'') \right] \exp \left\{ j \vec{q}'' \cdot \vec{r}'' - j \frac{k r''^2}{2r} [1 - \hat{s}'' \cdot \hat{r}'']^2 \right\} d\vec{r}'' \\ &= I_{d1} + I_{d2} \end{aligned} \quad (\text{A.1})$$

where $1 + \frac{(\hat{s}'' \cdot \vec{r}'')}{r}$ has been rewritten as $1 + \frac{r''}{r} (\hat{s}'' \cdot \hat{r}'')$ and

$$\begin{aligned}
 I_{d1} &= \int_{V''} \exp \left\{ j\bar{q}'' \cdot \bar{r}'' - j\frac{kr''^2}{2r} [1 - (\hat{s}'' \cdot \hat{r}'')^2] \right\} d\bar{r}'' \\
 I_{d2} &= \int_{V''} \frac{r''}{r} (\hat{s}'' \cdot \hat{r}'') \exp \left\{ j\bar{q}'' \cdot \bar{r}'' - j\frac{kr''^2}{2r} [1 - (\hat{s}'' \cdot \hat{r}'')^2] \right\} d\bar{r}''
 \end{aligned} \tag{A.2}$$

For a very thin disk, \bar{r}'' can be approximated by $\bar{r}'' \approx \rho''(\cos \phi'' \hat{x}'' + \sin \phi'' \hat{y}'')$ and $\bar{q}'' \cdot \bar{r}'' = \rho''(q_x'' \cos \phi'' + q_y'' \sin \phi'')$, $\hat{s}'' \cdot \hat{r}'' = s_x'' \cos \phi'' + s_y'' \sin \phi''$. Substituting these expressions into (A.2) and carrying out the integration with respect to the thickness of the disk, the integrals can be simplified to be

$$\begin{aligned}
 I_{d1} &= t \int_0^{2\pi} \int_0^a \rho'' g(\rho'', \phi'') d\rho'' d\phi'' \\
 I_{d2} &= t \int_0^{2\pi} \frac{1}{r} (s_x'' \cos \phi'' + s_y'' \sin \phi'') \int_0^a \rho''^2 g(\rho'', \phi'') d\rho'' d\phi''
 \end{aligned} \tag{A.3}$$

where the function $g(\rho'', \phi'')$ is given by

$$\begin{aligned}
 g(\rho'', \phi'') &= \exp \left\{ j\rho''(q_x'' \cos \phi'' + q_y'' \sin \phi'') - \right. \\
 &\quad \left. j\frac{k\rho''^2}{2r} [1 - (s_x'' \cos \phi'' + s_y'' \sin \phi'')^2] \right\} \\
 &= \exp [j\rho'' q_d - j(m_d \rho''^2 / 2)]
 \end{aligned} \tag{A.4}$$

and $q_d = q_x'' \cos \phi'' + q_y'' \sin \phi''$ and $m_d = k[1 - (s_x'' \cos \phi'' + s_y'' \sin \phi'')^2] / r$.

The integration over the radial distance of the disk in (A.3) can then be written as

$$\begin{aligned}
 g_1(\phi'') &= \int_0^a \rho'' g(\rho'', \phi'') d\rho'' = \int_0^a \rho'' \exp \left[j\rho'' q_d - j\frac{m_d \rho''^2}{2} \right] d\rho'' \\
 g_2(\phi'') &= \int_0^a \rho''^2 g(\rho'', \phi'') d\rho'' = \int_0^a \rho''^2 \exp \left[j\rho'' q_d - j\frac{m_d \rho''^2}{2} \right] d\rho''
 \end{aligned} \tag{A.5}$$

and the final forms of $g_1(\phi'')$ and $g_2(\phi'')$ after integration are given by [10]

$$g_1(\phi'') = \frac{q_d}{m_d} \sqrt{\frac{\pi}{2jm_d}} \exp\left(\frac{jq_d^2}{2m_d}\right) \left\{ \operatorname{erf}\left(\sqrt{\frac{jm_d}{2}} \left[a - \frac{q_d}{m_d}\right]\right) - \operatorname{erf}\left(q_d \sqrt{\frac{j}{2m_d}}\right) \right\} + \frac{j}{m_d} \left\{ \exp\left[\frac{m_d a^2}{2j} + jq_d a\right] - 1 \right\} \quad (\text{A.6})$$

$$g_2(\phi'') = j \frac{m_d a + q_d}{m_d^2} \exp\left(jaq_d - j \frac{m_d a^2}{2}\right) - \frac{jq_d}{m_d^2} + \frac{q_d^2 - jm_d}{m_d^2} \exp\left(\frac{jq_d^2}{2m_d}\right) \left[\sqrt{\frac{\pi}{2jm_d}} \left\{ \operatorname{erf}\left(\sqrt{\frac{jm_d}{2}} \left[a - \frac{q_d}{m_d}\right]\right) - \operatorname{erf}\left(q_d \sqrt{\frac{j}{2m_d}}\right) \right\} \right] \quad (\text{A.7})$$

Numerical integration with respect to the angle ϕ'' can be carried out to give I_{d1} and I_{d2} as shown below:

$$I_{d1} = t \int_0^{2\pi} g_1(\phi'') d\phi'' \quad (\text{A.8})$$

$$I_{d2} = t \int_0^{2\pi} \frac{1}{r} (s''_x \cos \phi'' + s''_y \sin \phi'') g_2(\phi'') d\phi''$$

For needle-shaped scatterers, the integral term in (14) can be divided into two parts as shown below:

$$I_{needle} = \int_{V''} \left[1 + \frac{r''}{r} (\hat{s}'' \cdot \hat{r}'') \right] \exp \left\{ j\vec{q}'' \cdot \vec{r}'' - j \frac{kr''^2}{2r} [1 - (\hat{s}'' \cdot \hat{r}'')^2] \right\} d\vec{r}'' = I_{n1} + I_{n2} \quad (\text{A.9})$$

where $1 + \frac{r''}{r} (\hat{s}'' \cdot \hat{r}'')$ and

$$I_{n1} = \int_{V''} \exp \left\{ j\vec{q}'' \cdot \vec{r}'' - j \frac{kr''^2}{2r} [1 - (\hat{s}'' \cdot \hat{r}'')^2] \right\} d\vec{r}''$$

$$I_{n2} = \int_{V''} \frac{r''}{r} (\hat{s}'' \cdot \hat{r}'') \exp \left\{ j\vec{q}'' \cdot \vec{r}'' - j \frac{kr''^2}{2r} [1 - (\hat{s}'' \cdot \hat{r}'')^2] \right\} d\vec{r}'' \quad (\text{A.10})$$

For a needle with very small radius a , the integration over the azimuthal angle ϕ'' and radial distance ρ'' can be approximated by πa^2 . This leads to $\bar{r}'' = \hat{z}'' z''$, $\bar{q}'' \cdot \bar{r}'' = q_z'' z''$, $\hat{s}'' \cdot \hat{r}'' = s_z''$. Substituting these expressions into (A.10) to give

$$I_{n1} = \pi a^2 \int_{-L/2}^{L/2} g(z'') dz'', \quad I_{n2} = \pi a^2 \frac{s_z''}{r} \int_{-L/2}^{L/2} z'' g(z'') dz'' \quad (\text{A.11})$$

where

$$\begin{aligned} g(z'') &= \exp \left[j z'' q_z'' - j \frac{k z''^2}{2r} (1 - s_z''^2) \right] \\ &= \exp \left(j z'' q_z'' - j \frac{m_n z''^2}{2} \right) \\ m_n &= k(1 - s_z''^2)/r \end{aligned} \quad (\text{A.12})$$

and the limit of integration has been chosen to be from $-L/2$ to $L/2$ (0 to L in [10]). The final expressions of I_{n1} and I_{n2} after integration are given by

$$\begin{aligned} I_{n1} &= \pi a^2 \exp \left(\frac{j q_z''^2}{2m_n} \right) \sqrt{\frac{\pi}{m_n}} \left\{ f_c(b_1) + f_c(b_2) - j [f_s(b_1) + f_s(b_2)] \right\} \\ I_{n2} &= \frac{s_z'' q_z''}{r m_n} I_{n1} + \pi a^2 \frac{j s_z''}{r m_n} \left[\exp \left(\frac{m_n L^2}{8j} - \frac{L q_z''}{2j} \right) - \right. \\ &\quad \left. \exp \left(\frac{m_n L^2}{8j} + \frac{L q_z''}{2j} \right) \right] \end{aligned} \quad (\text{A.13})$$

where $f_c(\cdot)$, $f_s(\cdot)$ are the Fresnel cosine and sine integral functions, respectively and are defined as follows [17]

$$f_c(x) = \sqrt{\frac{2}{\pi}} \int_0^x \cos(t^2) dt, \quad f_s(x) = \sqrt{\frac{2}{\pi}} \int_0^x \sin(t^2) dt \quad (\text{A.14})$$

and $b_1 = \sqrt{\frac{m_n}{2}} \left(\frac{L}{2} - \frac{q_z''}{m_n} \right)$, $b_2 = \sqrt{\frac{m_n}{2}} \left(\frac{L}{2} + \frac{q_z''}{m_n} \right)$.

REFERENCES

1. Stratton, J. A., *Electromagnetic Theory*, McGraw-Hill, New York, 1941.
2. Van de Hulst, H. C., *Light Scattering by Small Particles*, John Wiley and Sons, New York, 1957.
3. Schiffer, R., and K. O. Thielheim, "Light scattering by dielectric needles and disks," *Journal of Applied Physics*, Vol. 50, No. 4, 2476–2483, 1979.
4. Karam, M. A., A. K. Fung, and Y. M. M. Antar, "Electromagnetic wave scattering from some vegetation samples," *IEEE Transactions on Geoscience and Remote Sensing*, Vol. 26, No. 6, 799–807, 1988.
5. Ruck, G. T., D. E. Barrick, W. D. Stuart, and C. K. Krichbaum, *Radar Cross Section Handbook*, Vol. 1, Plenum Press, New York, 1970.
6. Wait, J. R., "Scattering of a plane wave from a circular dielectric cylinder at oblique incidence," *Canadian Journal of Physics*, Vol. 33, 189–195, 1955.
7. Wait, J. R., *Electromagnetic Radiation from Cylindrical Structures*, Pergamon Press, New York, 1959.
8. Karam, M. A., and A. K. Fung, "Electromagnetic scattering from a layer of finite length, randomly oriented, dielectric, circular cylinders over a rough interface with application to vegetation," *International Journal of Remote Sensing*, Vol. 9, No. 6, 1109–1134, 1988.
9. Fung, A. K., M. F. Chen, and K. K. Lee, "Fresnel field application applied to scattering from a vegetation layer," *Remote Sensing of Environment*, Vol. 23, 35–50, 1987.
10. Fung, A. K., *Microwave Scattering and Emission Models and Their Applications*, Artech House, Norwood, Massachusetts, 1994.
11. Staelin, D. H., A. W. Morgenthaler, and J. A. Kong, *Electromagnetic Waves*, Prentice Hall, New Jersey, 1994.
12. Ishimaru, A., *Electromagnetic Wave Propagation, Radiation, and Scattering*, Prentice Hall, New Jersey, 1991.
13. Gradshteyn, I. S., and I. M. Ryzhik, *Table of Integrals, Series and Products*, Academic Press, New York, 1965.
14. Allan, L. E., and G. C. McCormick, "Measurements of the backscatter matrix of dielectric bodies," *IEEE Transactions on Antennas and Propagation*, Vol. 28, No. 2, 166–169, 1980.
15. Allan, L. E., and G. C. McCormick, "Measurements of the backscatter matrix of dielectric spheroids," *IEEE Transactions on Antennas and Propagation*, Vol. 26, No. 4, 579–587, 1978.

16. Ulaby, F. T., and M. A. El-Rayes, "Microwave dielectric spectrum of vegetation Part II: Dual dispersion model," *IEEE Transactions on Geoscience and Remote Sensing*, Vol. 25, No. 5, 550–557, 1987.
17. Abramowitz, M., and I. A. Stegun, (Eds.), *Handbook of Mathematical Functions*, Dover, New York, 1970